

# Bell Inequalities and Quantum Correlations in $H \rightarrow ZZ \rightarrow 2e 2\mu$

Mira Varma and Oliver K. Baker

Department of Physics, Yale University, New Haven, CT 06520, USA

mira.varma@yale.edu

February 5, 2025

## Abstract

We investigate quantum correlations in Higgs-boson decays ( $H \rightarrow ZZ^* \rightarrow 2e 2\mu$ ) using CMS open data at  $\sqrt{s} = 8$  TeV, incorporating realistic detector effects. By reconstructing the polarization density matrix of the two-boson system and evaluating the Collins-Gisin-Linden-Massar-Popescu (CGLMP) Bell operator  $I_3$ , we quantify entanglement in the  $ZZ$  state. Our analysis shows that 90.7% of signal events ( $H \rightarrow ZZ^*$ ) violate the Bell inequality ( $I_3 > 2$ ), indicating strong quantum correlations, while only 11.8% of non-resonant continuum background events ( $pp \rightarrow ZZ$ ) exhibit such a violation. These results demonstrate the feasibility of testing fundamental quantum mechanics at high energy colliders.

## 1 Introduction

Quantum entanglement, a phenomenon at the heart of quantum mechanics [1, 2], has been extensively explored at low energies in systems such as photons [3], trapped ions [4], and superconducting qubits [5]. Only recently has it emerged as a powerful tool for probing particle interactions at much higher energies. This paper investigates quantum entanglement in the context of the Large Hadron Collider (LHC), pushing our understanding of this quintessential quantum effect to unprecedented energy scales<sup>1</sup>.

As Schrödinger once noted, entanglement is “not one but rather the characteristic trait of quantum mechanics” [7]. By studying entanglement at the LHC, we hope to leverage this key phenomenon to gain new insights into high-energy particle physics. Recent results from ATLAS [8] and CMS [9] have provided the first evidence of entanglement in top-quark pair production at the LHC. This follows earlier observations of Bell inequality violations [10]—fundamental tests of quantum correlations rooted in the Einstein-Podolsky-Rosen completeness paradox [11]—in particle physics using B-meson decays at LHCb and Belle II [12]. These results demonstrate that quantum correlations persist at energies over

<sup>1</sup>For a recent comprehensive review of entanglement and Bell tests in high-energy collisions, see [6]

12 orders of magnitude [3, 13, 14, 15] higher than those in typical laboratory entanglement experiments.

Building on this foundation, we extend the study of quantum entanglement to the Higgs sector, focusing on the decay channel  $H \rightarrow ZZ^* \rightarrow 2e2\mu$ , with the  $pp \rightarrow ZZ$  process serving as the primary background. Recent theoretical work suggests this channel is particularly promising for observing Bell inequality violations [16, 17], with predictions pointing toward potential observations at the HL-LHC. The four-lepton final state offers a clean experimental signature [18] where the complete kinematics can be reconstructed, making it ideal for quantum state analysis [19, 20].

The theoretical framework for analyzing entanglement in  $H \rightarrow ZZ^*$  has been developed in several recent papers. The construction of the appropriate Bell operators was outlined in [16], while comprehensive analytical predictions for the polarization density matrix were provided in [21]. The quantum tomography techniques required for reconstructing density matrices from experimental data were detailed in [17]. For related proposals to perform quantum tomography in collider physics, see Refs. [22, 23, 24], which focus on top-quark pair production and spin-state reconstruction using quantum-information methods.

In our approach, we employ the polarization density matrix reconstruction technique developed by [21] using CMS open data. This marks the first attempt to apply these theoretical methods to  $H \rightarrow ZZ \rightarrow 4\ell$  collider data that includes detector effects. By computing the Bell operator expectation value  $I_3$ , we aim to quantify the quantum correlations in these high-energy processes and test this important aspect of quantum mechanics at collider energies.

This work has the potential to:

1. Extend our understanding of quantum entanglement to unprecedented energies,
2. Provide new tests of quantum mechanics in extreme environments,
3. Offer novel probes of the Higgs boson's properties and interactions, and
4. Bridge the gap between quantum information theory and high-energy particle physics.

Whereas previous studies have been either purely theoretical or based on truth-level Monte Carlo simulations, this work demonstrates the feasibility of reconstructing the polarization density matrix using simulated data that includes detector effects. Although using an outreach dataset limits the statistical precision possible, successfully implementing these techniques with detector-level events represents an important step toward future measurements of quantum correlations in the Higgs sector using actual collision data.

## 2 Background

Our work leverages the fact that massive spin-1 bosons, like the  $Z$ -bosons produced in Higgs decays or non-resonant di-boson processes, can exhibit quantum correlations beyond any classical description. We adopt the density matrix formalism, using simulation-level data that include realistic detector effects—making our analysis especially relevant for experimental high-energy physics. While some earlier studies rely on truth-level data alone, we account for the complexities introduced by the detector.

## 2.1 Quantum State of the Di-boson System

When a Higgs boson decays into two  $Z$ -bosons, the resulting  $ZZ^*$  is produced in a singlet state. This state can be written as:

$$|\Psi\rangle = \frac{1}{\sqrt{3}} (|1, -1\rangle - |0, 0\rangle + |-1, 1\rangle), \quad (1)$$

where  $(+1, 0, -1)$  denote the helicities of the two  $Z$ -bosons. This superposition describes maximal entanglement in the system, in which the spin states of the two bosons are perfectly correlated.

In this work, we focus on the  $2e2\mu$  decay channel. This choice provides an extra layer of clarity: each flavor pair (electrons or muons) must come from its respective  $Z$ -boson, thus minimizing ambiguities in pairing leptons. Observing one lepton effectively identifies its parent  $Z$ , enabling us to infer properties of the corresponding second boson via conservation of quantum numbers.

## 2.2 The Density Matrix Formalism

### 2.2.1 Single-Boson Polarization Density Matrix

A single massive spin-1 boson, such as the  $Z$ , can be described by a  $3 \times 3$  polarization density matrix,  $\rho$ . A spin-1 particle has three possible helicity states  $\lambda \in \{+1, 0, -1\}$ , which describe the projection of its spin onto a chosen axis. The elements of the density matrix are:

$$\rho_{\lambda\lambda'} = \frac{\mathcal{M}(\lambda)\mathcal{M}^*(\lambda')}{\sum_{\lambda} |\mathcal{M}(\lambda)|^2}, \quad (2)$$

where  $\mathcal{M}(\lambda)$  is the helicity amplitude for the given state.  $\lambda, \lambda' \in \{-1, 0, +1\}$ . The diagonal entries  $\rho_{\lambda\lambda}$  represent the probabilities of the boson being in a given helicity state, while off-diagonal elements ( $\lambda \neq \lambda'$ ) encode quantum coherence. These off-diagonal terms are particularly important, as they reveal quantum correlations within the system.

### 2.2.2 Two-Boson Density Matrix

When two spin-1 bosons (e.g.,  $Z$ -bosons) appear simultaneously, such as in  $H \rightarrow ZZ^*$  or non-resonant  $ZZ$  production, their joint quantum state resides in a  $3 \otimes 3$  Hilbert space, described by a  $9 \times 9$  density matrix  $\rho_{(2)}$ .<sup>2</sup> One can expand in terms of the Gell-Mann basis ( $T^a, a = 1, \dots, 8$ ) and the identity matrix  $\mathbb{I}$ :

$$\rho_{(2)} = \left( \frac{1}{9} [\mathbb{I} \otimes \mathbb{I}] + \sum_{a=1}^8 f_a [T^a \otimes \mathbb{I}] + \sum_{b=1}^8 g_b [\mathbb{I} \otimes T^b] + \sum_{a,b=1}^8 h_{ab} [T^a \otimes T^b] \right)_{\lambda_1, \lambda'_1, \lambda_2, \lambda'_2}. \quad (3)$$

The real coefficients  $f_a$ ,  $g_b$ , and  $h_{ab}$  describe all single- and double-polarization observables. Off-diagonal elements in  $\rho_{(2)}$  encode quantum correlations, including entanglement.

<sup>2</sup>See Refs. [25, 26, 16] for related discussions of spin-1 entangled states in collider processes.

For  $H \rightarrow ZZ^*$ , the key non-zero elements are:

$$\begin{aligned} h_{16} = h_{61} = h_{27} = h_{72} &= \frac{fM_V^2[-m_H^2 + (1+f^2)M_V^2]}{D}, \\ h_{33} &= \frac{1[m_H^2 - (1+f^2)M_V^2]^2}{4D}, \\ h_{44} &= \frac{2f^2M_V^4}{D}, \end{aligned} \tag{4}$$

where,

- $f = M_Z^*/M_Z$  is the mass ratio of the off-shell to on-shell  $Z$ -boson
- $D = m_H^4 - 2(1+f^2)m_H^2M_V^2 + (1+10f^2+f^4)M_V^4$  is the denominator
- $M_V^2$  represents the vector (in this case  $Z$ ) boson mass

### 2.3 Bell Inequalities for Spin-1 Particles

In the case of two spin-1 particles, we can employ the Collins–Gisin–Linden–Massar–Popescu inequality [27, 28], which extends Bell tests to three-level (qutrit) systems. Its associated Bell observable,  $I_3$ , is computed via polarization density matrix coefficients.

1. If  $I_3 \leq 2$ , the correlations in can be explained by local hidden-variable models, suggesting quantum mechanics may be incomplete.
2. If  $I_3 > 2$ , the Bell inequality is violated, indicating quantum entanglement.

Our study finds  $I_3 > 2$  predominantly in Higgs-mediated ( $H \rightarrow ZZ^*$ ) processes, while the continuum  $ZZ$  background rarely exceeds this threshold. Since we work at detector level, these results are particularly relevant to potential future experimental measurements.

#### 2.3.1 Bell’s Inequality from Density Matrix Coefficients

In our formalism, the CGLMP operator  $I_3$  is defined in terms of the density matrix coefficients [21]:

$$I_3 = 4(h_{44} + h_{55}) - \frac{4\sqrt{3}}{3}[h_{61} + h_{66} + h_{72} + h_{77} + h_{11} + h_{16} + h_{22} + h_{27}] \tag{5}$$

The general form of the Bell operator  $I_3$  can be simplified using symmetries of the  $H \rightarrow ZZ^*$  system. From the symmetries of the decay, we have  $h_{16} = h_{61} = h_{27} = h_{72}$ ,  $h_{38} = h_{83}$ , and  $h_{44} = h_{55}$ . Substituting these relations into the above equation gives us the simplified expression for  $I_3$  [21]:

$$I_3 = 8h_{44} - \frac{16}{\sqrt{3}}h_{16} \tag{6}$$

## 2.4 Reconstruction from Lepton Decay Angles

When each  $Z$ -boson decays to a lepton pair, the resulting daughter particles ( $\ell^+\ell^-$ ) encode spin information about the original boson. We reconstruct their four-momenta in the lab frame using standard formulas<sup>3</sup>:

$$\begin{aligned} p_x &= p_T \cos(\phi) \\ p_y &= p_T \sin(\phi) \\ p_z &= p_T \sinh(\eta) \\ E &= \sqrt{p_x^2 + p_y^2 + p_z^2 + m^2}. \end{aligned} \tag{7}$$

We then boost into the Higgs rest frame to identify  $Z$ -boson momenta:

$$p_{Z1} = p_{\ell1} + p_{\ell2}, \quad p_{Z2} = p_{\ell3} + p_{\ell4}.$$

From these momenta, we compute the invariant masses  $m_{Z1}$  and  $m_{Z2}$ . To reconstruct the polarization density matrix, the only experimental input we need is the ratio  $f$ :

$$f = \frac{m_{Z2}}{m_{Z1}}. \tag{8}$$

Boosting further into each  $Z$  rest frame, we obtain the polar ( $\theta$ ) and azimuthal ( $\phi$ ) angles of the negatively charged lepton:

$$\theta_{Z_{1,2}} = \arccos \left( \frac{p_{z_{Z_{1,2}}}}{\sqrt{p_{x_{Z_{1,2}}}^2 + p_{y_{Z_{1,2}}}^2 + p_{z_{Z_{1,2}}}^2}} \right), \quad \phi_{Z_{1,2}} = \arctan \left( \frac{p_{y_{Z_{1,2}}}}{p_{x_{Z_{1,2}}}} \right),$$

where the momenta components are those of the negatively charged leptons in their respective parent  $Z$ -boson rest frames.

## 3 Data and Methodology

We analyze publicly available CMS Open Data [30, 31] at  $\sqrt{s} = 8$  TeV, containing both Higgs boson decays and non-resonant  $ZZ^*$  production under realistic detector conditions.<sup>4</sup>

For the signal, we analyzed  $H \rightarrow ZZ^* \rightarrow 4\ell$  events, where the final-state leptons consisted of two electrons and two muons ( $2e2\mu$ ). This final state was chosen to avoid ambiguities in identifying which leptons originated from which  $Z$ -boson, an issue that arises in events with four same-flavor leptons. Events were generated using the POWHEG event generator, with PYTHIA6 applied for parton showering. The full dataset contained 299,973 events, of which 27,945 were analyzed to ensure a balanced comparison with the filtered background dataset, described below.

<sup>3</sup>If one is unfamiliar with these relations, Ref. [29] is an excellent resource.

<sup>4</sup>These datasets were derived from primary CMS datasets in AOD format, which were validated by the CMS collaboration. The reduced NanoAOD format retains key kinematic and detector-level information and has been optimized for education and outreach purposes.

For the background, we considered non-resonant  $ZZ^* \rightarrow 4\ell$  production ( $pp \rightarrow ZZ^* \rightarrow 4\ell$ ) under identical simulation conditions. This process constitutes the primary background for  $H \rightarrow ZZ^* \rightarrow 4\ell$ , as it produces the same final state without involving an intermediate Higgs boson. The dataset included 1,497,445 events, focusing on the same  $2e2\mu$  final state as the signal.

To isolate events consistent with the  $H \rightarrow ZZ^* \rightarrow 4\ell$  process and the  $ZZ^*$  background, we applied a filtering criterion based on the sum of the invariant masses of the two  $Z$ -bosons:

$$120 \text{ GeV} \leq M_{Z_1} + M_{Z_2} \leq 130 \text{ GeV}.$$

This filter was chosen to isolate events consistent with the kinematics of  $H \rightarrow ZZ^* \rightarrow 4\ell$  decays, as the Higgs boson mass is approximately 125 GeV. Since the background dataset represents non-resonant  $ZZ^*$  production, it contains events across a wide range of kinematics. The filter suppresses contributions from events outside the Higgs mass range, ensuring that the remaining background events closely resemble those expected in Higgs decays. The filtering criterion was applied uniformly to both the signal and background datasets to isolate events consistent with the expected kinematics of  $H \rightarrow ZZ^* \rightarrow 4\ell$  decays. All results presented in this paper use this  $Z$ -boson sum mass selection criterion. An alternative selection based on the Higgs mass ( $120 \text{ GeV} \leq m_H \leq 130 \text{ GeV}$ ) was explored but found to produce less consistent results. We instead chose the  $Z$ -boson sum mass criterion due to its direct connection to the quantum correlations we aim to study.

## 4 Results

### 4.1 Bell Operator $I_3$ Distributions

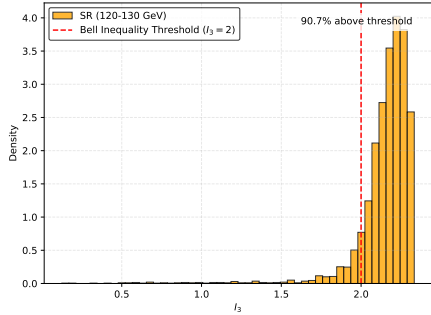
Figure 1 shows the distribution of  $I_3$  for signal (orange) and background (blue). For the signal dataset, 90.7% exceed  $I_3 > 2$ , with an average of  $2.152 \pm 0.003$ . In contrast, only 11.8% of background events do so, averaging  $1.158 \pm 0.012$ . The stark difference between these two values reinforces the presence of entanglement in the Higgs-mediated channel.

### 4.2 Angular Distributions and Correlations

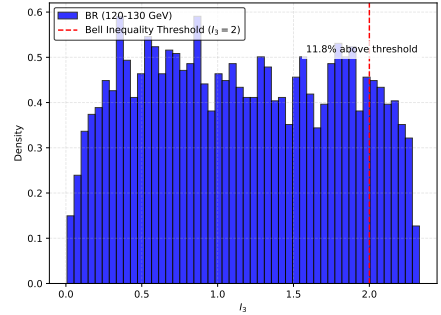
Figure 2 presents the polar ( $\theta_{Z_1}, \theta_{Z_2}$ ) and azimuthal ( $\phi_{Z_1}, \phi_{Z_2}$ ) distributions for both signal and background. The polar angles exhibit broad peaks between  $75^\circ$  and  $100^\circ$ , diminishing near  $0^\circ$  or  $180^\circ$ . The azimuthal angles appear nearly uniform. The azimuthal angle distributions remain approximately uniform over the range  $-180^\circ$  to  $180^\circ$  for both samples.

The dependence of the Bell operator  $I_3$  on these angular variables was also examined (Fig. 3) to identify possible angular effects on Bell inequality violation. For the signal dataset, strong violations of the Bell inequality ( $I_3 > 2$ ) are observed across all angular ranges. However, slight reductions in  $I_3$  values are present near the polar angle extremes. No such reduction is observed for the azimuthal angles, where  $I_3$  values remain uniform across the range.

The background events, however, display  $I_3$  values ranging from 0 to approximately 2.2, showing no significant correlation with any angular variables.



(a)



(b)

Figure 1: Distribution of the Bell operator  $I_3$  for (a) signal and (b) background events in the 120–130 GeV mass window. Signal events show significant Bell inequality violations ( $I_3 > 2$ ), with 90.7% exceeding the threshold, while background events remain predominantly below the threshold (11.8% violation rate).

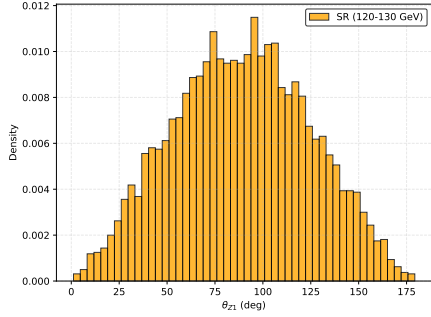
### 4.3 Mass Distributions and Bell Operator Correlations

Figure 5 illustrates the dependence of the Bell operator  $I_3$  on kinematic variables ( $m_{ZZ}$ ,  $m_{ZZ}$ , and  $p_T^{miss}$ ). Signal events consistently exhibit  $I_3 > 2$ , with a higher density observed at  $m_{ZZ}$  between 20 GeV and 40 GeV, and clustering at  $m_{ZZ}$  in the range 87 GeV to 95 GeV. Background events remain below the threshold, showing no significant correlation with these variables.

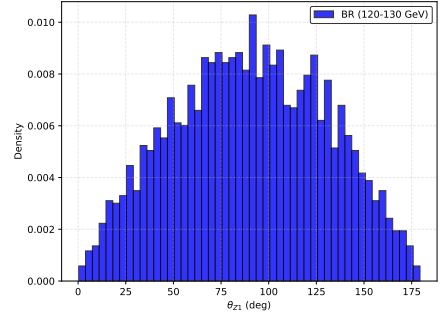
The variation of  $I_3$  with missing transverse momentum ( $p_T^{miss}$ ) is also shown in Figure 5. Signal events show  $I_3 > 2$  across the entire  $p_T^{miss}$  range, with a higher density of violations for  $p_T^{miss} \leq 30$  GeV. Background events maintain consistently low  $I_3$  values regardless of  $p_T^{miss}$ , further highlighting the absence of quantum correlations in non-signal processes.

### 4.4 Density Matrices for Signal and Background Samples

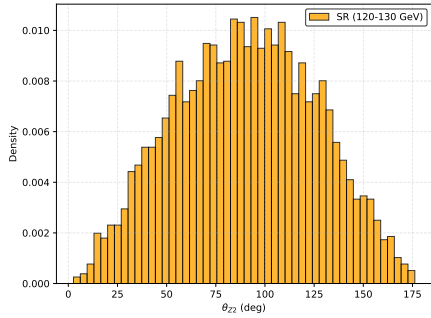
After aggregating events in the  $120 \text{ GeV} \leq m_{ZZ} \leq 130 \text{ GeV}$  window, we average over all reconstructed events to obtain the final density matrices. Below are the numerical results for the signal channel ( $H \rightarrow ZZ^*$ ) and the continuum background ( $pp \rightarrow ZZ^*$ ). These matrices are written in the helicity basis  $\{|+1, +1\rangle, |+1, 0\rangle, \dots, |-1, -1\rangle\}$  with indices running from 1 to 9. The magnitude of off-diagonal elements indicates the strength of quantum correlations between the Z bosons, with larger values in the signal suggesting stronger entanglement.



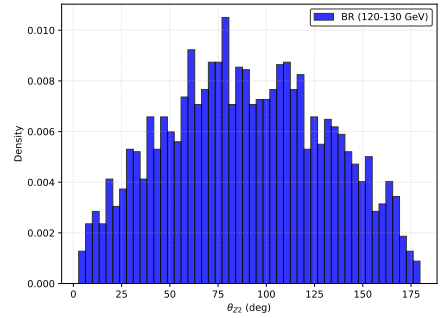
(a)



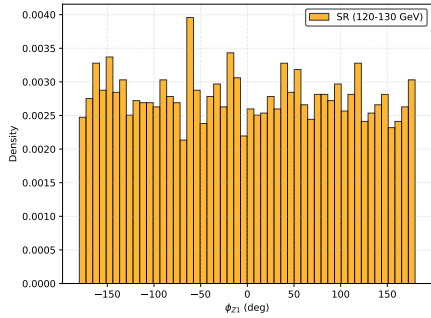
(b)



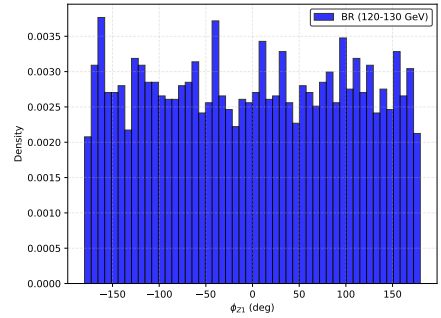
(c)



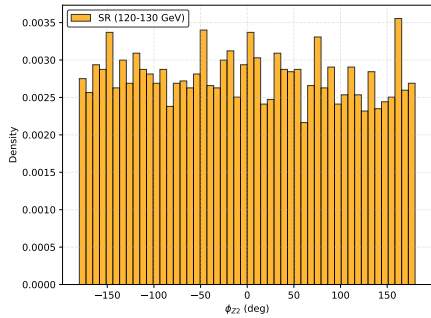
(d)



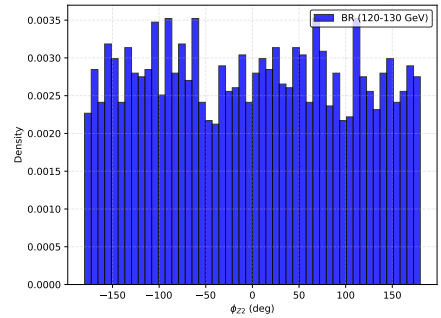
(e)



(f)



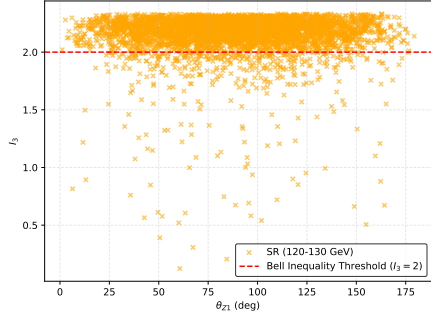
(g)



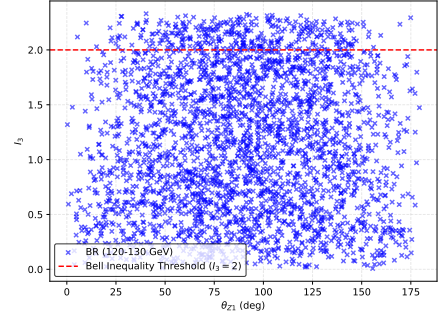
(h)

Figure 2: Angular distributions for signal (orange) and background (blue) events in the mass window  $120 \text{ GeV} \leq m_{ZZ} \leq 130 \text{ GeV}$ . Top row: polar angle distributions for (a)  $\theta_{Z1}$  signal, (b)  $\theta_{Z1}$  background, (c)  $\theta_{Z2}$  signal, and (d)  $\theta_{Z2}$  background. Bottom row: azimuthal angle distributions for (e)  $\phi_{Z1}$  signal, (f)  $\phi_{Z1}$  background, (g)  $\phi_{Z2}$  signal, and (h)  $\phi_{Z2}$  background.

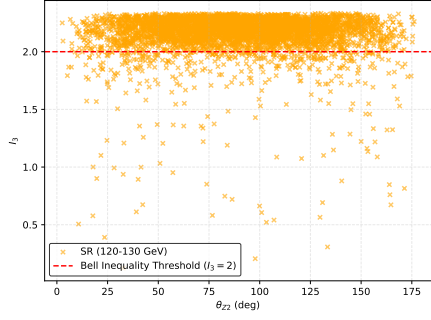




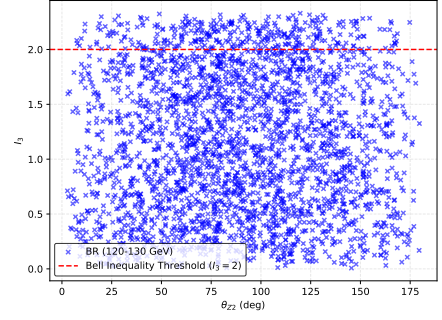
(a)



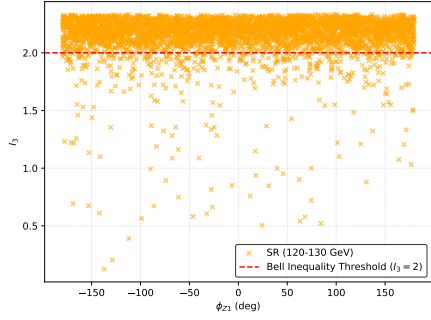
(b)



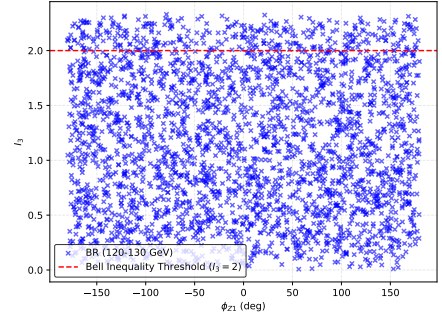
(c)



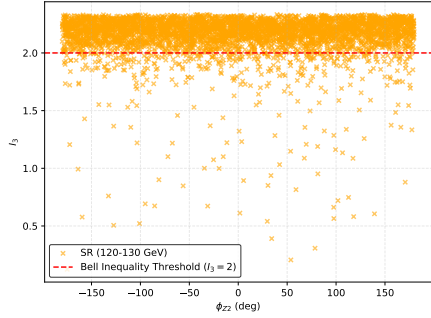
(d)



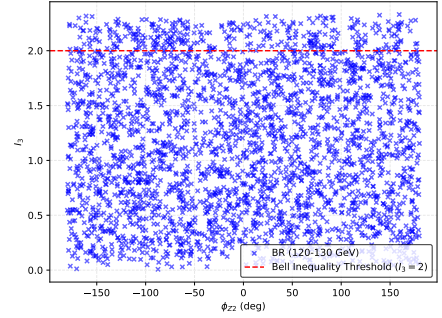
(e)



(f)

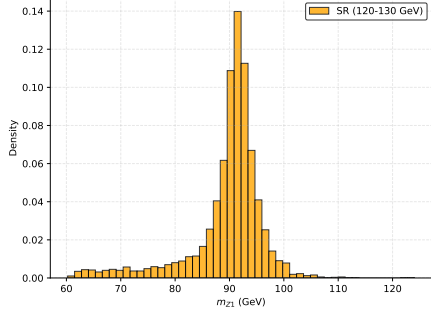


(g)

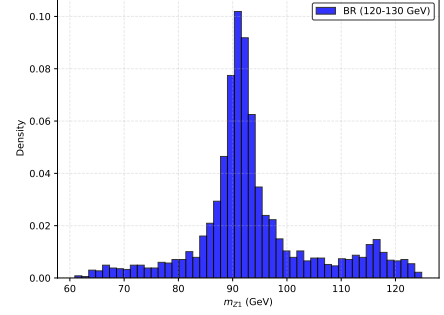


(h)

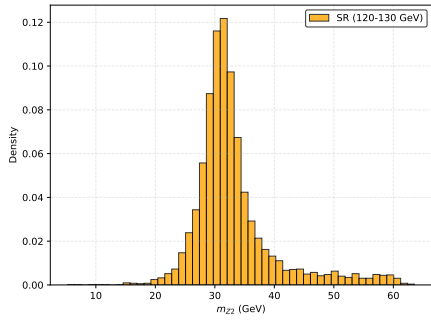
Figure 3: Bell operator  $I_3$  correlations with angular variables for signal (orange) and background (blue) events. The red dashed line indicates the Bell inequality threshold ( $I_3 = 2$ ). Correlation with polar angles: (a)  $\theta_{Z1}$  signal, (b)  $\theta_{Z1}$  background, (c)  $\theta_{Z2}$  signal, (d)  $\theta_{Z2}$  background. Correlation with azimuthal angles: (e)  $\phi_{Z1}$  signal, (f)  $\phi_{Z1}$  background, (g)  $\phi_{Z2}$  signal, (h)  $\phi_{Z2}$  background.



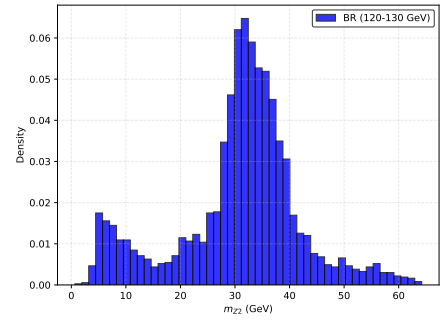
(a)



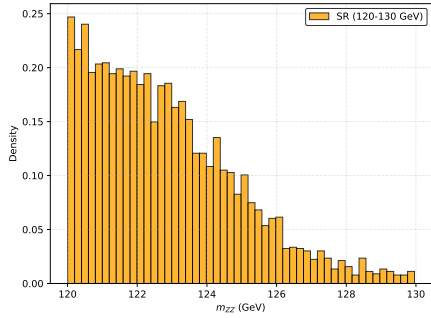
(b)



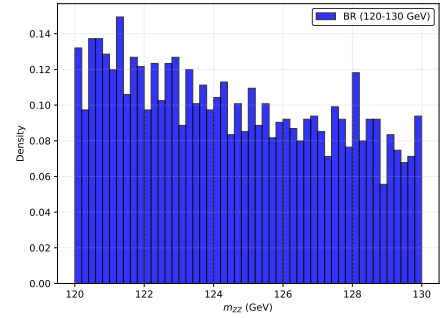
(c)



(d)



(e)



(f)

Figure 4: Mass distributions in the  $120 \text{ GeV} \leq m_{ZZ} \leq 130 \text{ GeV}$  window. On-shell  $Z$ -boson mass ( $m_{Z1}$ ) for (a) signal ( $\langle m_{Z1} \rangle = 89.67 \pm 0.10 \text{ GeV}$ ) and (b) background ( $\langle m_{Z1} \rangle = 93.72 \pm 0.21 \text{ GeV}$ ). Off-shell  $Z$ -boson mass ( $m_{Z2}$ ) for (c) signal ( $\langle m_{Z2} \rangle = 33.14 \pm 0.10 \text{ GeV}$ ) and (d) background ( $\langle m_{Z2} \rangle = 30.83 \pm 0.21 \text{ GeV}$ ). Four-lepton invariant mass ( $m_{ZZ}$ ) for (e) signal ( $\langle m_{ZZ} \rangle = 122.81 \pm 0.14 \text{ GeV}$ ) and (f) background ( $\langle m_{ZZ} \rangle = 124.54 \pm 0.30 \text{ GeV}$ ).

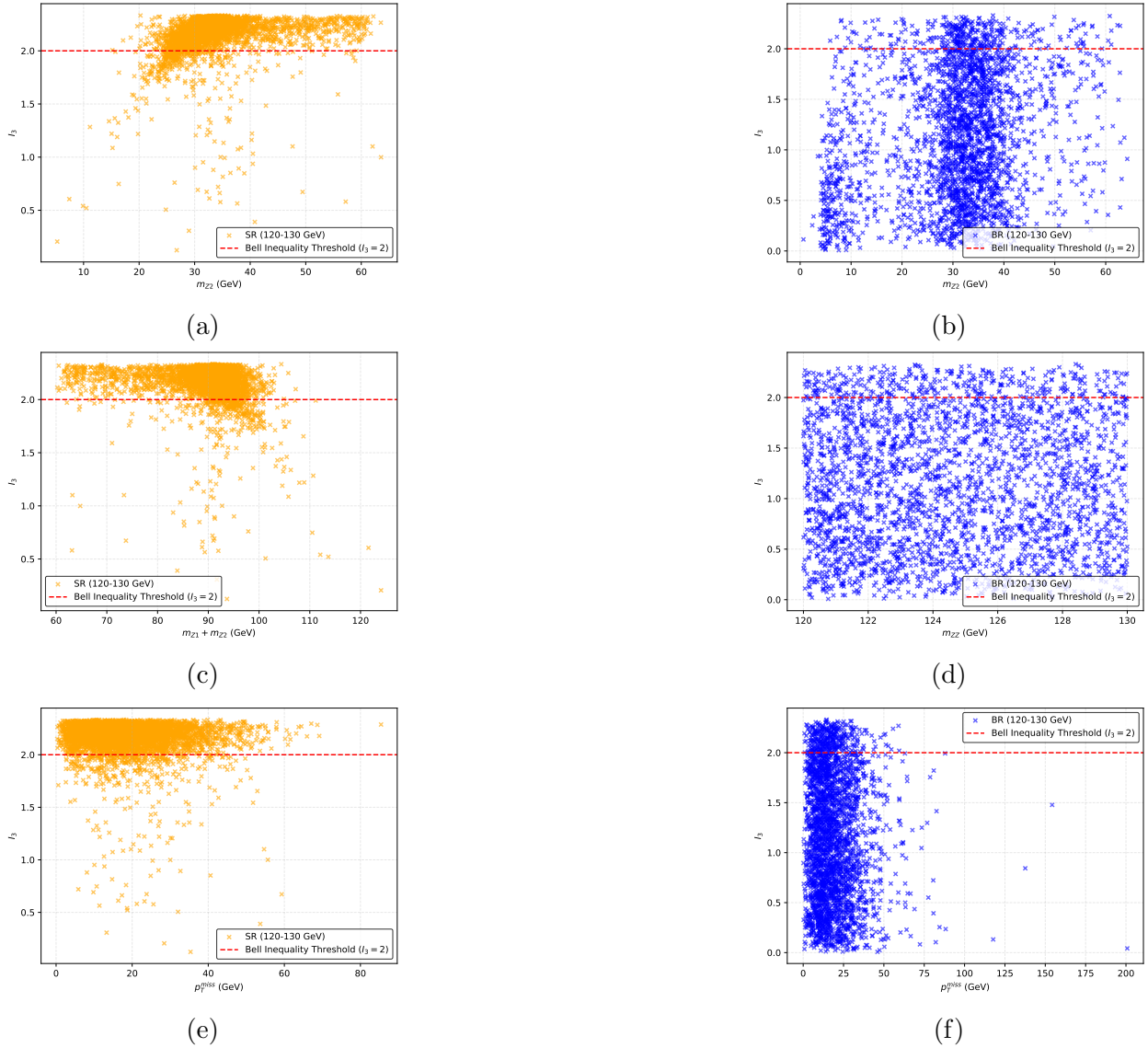


Figure 5: Bell operator  $I_3$  dependence on kinematic variables for signal (orange) and background (blue) events. The red dashed line indicates  $I_3 = 2$ . (a,b)  $I_3$  versus  $m_{Z2}$ , showing signal clustering at 20–40 GeV. (c,d)  $I_3$  versus  $m_{ZZ}$ , with strong violations at 87–95 GeV. (e,f)  $I_3$  versus  $p_T^{\text{miss}}$ , with signal events maintaining  $I_3 > 2$  and clustering below 30 GeV.

**Signal Matrix ( $\rho_{\text{signal}}$ ):**

$$\rho_{\text{signal}} = 2 \begin{pmatrix} 0 & 0 & 0 & 0 & 0 & 0 & 0 & 0 & 0 \\ 0 & 0 & 0 & 0 & 0 & 0 & 0 & 0 & 0 \\ 0 & 0 & 0.1058 & 0 & -0.2448 & 0 & 0.1058 & 0 & 0 \\ 0 & 0 & 0 & 0 & 0 & 0 & 0 & 0 & 0 \\ 0 & 0 & -0.2448 & 0 & 0.2884 & 0 & -0.2448 & 0 & 0 \\ 0 & 0 & 0 & 0 & 0 & 0 & 0 & 0 & 0 \\ 0 & 0 & 0.1058 & 0 & -0.2448 & 0 & 0.1058 & 0 & 0 \\ 0 & 0 & 0 & 0 & 0 & 0 & 0 & 0 & 0 \\ 0 & 0 & 0 & 0 & 0 & 0 & 0 & 0 & 0 \end{pmatrix}. \quad (9)$$

**Background Matrix ( $\rho_{\text{bkg}}$ ):**

$$\rho_{\text{bkg}} = 2 \begin{pmatrix} 0 & 0 & 0 & 0 & 0 & 0 & 0 & 0 & 0 \\ 0 & 0 & 0 & 0 & 0 & 0 & 0 & 0 & 0 \\ 0 & 0 & 0.0405 & 0 & -0.1563 & 0 & 0.0405 & 0 & 0 \\ 0 & 0 & 0 & 0 & 0 & 0 & 0 & 0 & 0 \\ 0 & 0 & -0.1563 & 0 & 0.4189 & 0 & -0.1563 & 0 & 0 \\ 0 & 0 & 0 & 0 & 0 & 0 & 0 & 0 & 0 \\ 0 & 0 & 0.0405 & 0 & -0.1563 & 0 & 0.0405 & 0 & 0 \\ 0 & 0 & 0 & 0 & 0 & 0 & 0 & 0 & 0 \\ 0 & 0 & 0 & 0 & 0 & 0 & 0 & 0 & 0 \end{pmatrix}. \quad (10)$$

Following the standard convention for spin-1 entangled systems [21], we multiply the reconstructed density matrices by a factor of 2 to ensure this normalization in the helicity basis. For the  $Z_1 + Z_2$  mass filtering, the averaged density matrix was found to satisfy  $\text{Tr}(\rho) = 1$ , indicating proper normalization and a consistent quantum state representation.

In contrast, alternative filtering methods, such as Higgs mass filtering, produced  $\text{Tr}(\rho) \neq 1$ , highlighting the reliability of the  $Z_1 + Z_2$  mass filtering. The off-diagonal elements, representing quantum coherence, are significantly larger for the signal sample, reflecting the presence of strong quantum entanglement in  $H \rightarrow ZZ^* \rightarrow 4\ell$  decays. This quantum coherence is absent in the background, highlighting the fundamental differences between resonant Higgs production and non-resonant di-boson processes.

## 4.5 Interpretation of Off-Diagonal Elements

The non-zero off-diagonal elements in the density matrices quantify quantum correlations between different helicity states of the  $Z$  bosons. In the signal sample, these elements are larger because the spin-0 Higgs boson must decay to a specific quantum superposition of  $ZZ^*$  helicity states to conserve angular momentum. Comparing the matrices, we observe that the off-diagonal elements in the signal are approximately twice the magnitude of those in the background, indicating stronger entanglement between the  $Z$  bosons in Higgs decays. The smaller off-diagonal elements in the background process occur since the  $Z$  bosons are produced directly in  $pp$  collisions without constraints from an intermediate resonance, resulting in weaker quantum correlations.

## 4.6 Statistical Uncertainties

The statistical uncertainties on the non-zero elements of  $\rho_{\text{signal}}$  are:

- $\rho_{2,3} = \rho_{2,7} = \rho_{7,3} = \rho_{7,7} = 0.105805 \pm 0.000225$
- $\rho_{2,5} = \rho_{5,2} = \rho_{5,7} = \rho_{7,5} = -0.244798 \pm 0.000208$
- $\rho_{5,5} = 0.28839 \pm 0.000225$

Similarly, for  $\rho_{\text{bkg}}$ :

- $\rho_{2,3} = \rho_{2,7} = \rho_{7,3} = \rho_{7,7} = 0.040539 \pm 0.000635$
- $\rho_{2,5} = \rho_{5,2} = \rho_{5,7} = \rho_{7,5} = -0.156318 \pm 0.001303$
- $\rho_{5,5} = 0.418922 \pm 0.000635$

## 5 Discussion

This study demonstrates significant violations of the Bell inequality in  $H \rightarrow ZZ^* \rightarrow 4\ell$  decays, as evidenced by the distribution of the Bell operator  $I_3$ . The finding that 90.7% of signal events exceed the Bell inequality threshold ( $I_3 > 2$ ) provides strong evidence for the presence of quantum entanglement in this process, even in the presence of detector effects.

The effectiveness of the  $Z_1 + Z_2$  mass filtering arises from its direct connection to the  $ZZ^*$  system kinematics. By selecting events based on the sum of  $Z$ -boson masses, we better isolate signal events from background processes, as evidenced by the proper normalization  $\text{Tr}(\rho) = 1$  and the clear separation between signal and background quantum correlations. This is particularly apparent in the density matrix off-diagonal elements, which are significantly larger for the signal sample, reflecting the strong quantum entanglement expected in Higgs-mediated decays.

The angular dependence of  $I_3$  reveals notable differences. Polar angles ( $\theta_{Z1}, \theta_{Z2}$ ) show a slight reduction in  $I_3$  near the extremes, possibly reflecting spin correlations in the Higgs rest frame. Azimuthal angles ( $\phi_{Z1}, \phi_{Z2}$ ) show no such dependence, suggesting that these angles are less sensitive to spin effects.

The clustering of  $I_3 > 2$  events in specific mass ranges (e.g., 20–40 GeV for  $m_{Z2}$  and 87–95 GeV for  $m_{ZZ}$ ) underscores regions of heightened quantum correlations. These patterns are absent in the background, emphasizing sensitivity to entanglement in the signal process. While this analysis focuses on statistical uncertainties, several systematic effects could influence these measurements, including detector resolution and acceptance effects in lepton reconstruction, and uncertainties in background modeling. A detailed study of these systematic uncertainties and their impact on density matrix reconstruction is beyond the scope of this paper but will be important for future measurements with collision data.

## 6 Conclusion

In this work, we have reconstructed the polarization density matrix for both the signal channel ( $H \rightarrow ZZ^* \rightarrow 4\ell$ ) and the non-resonant continuum background ( $pp \rightarrow ZZ^* \rightarrow 4\ell$ ) using CMS open source data that incorporates realistic detector effects. Focusing on the mass window  $120 \text{ GeV} \leq m_{ZZ} \leq 130 \text{ GeV}$ , our results indicate that 90.7% of the signal events exceed the Bell-inequality threshold  $I_3 = 2$ , while only 11.8% of background events do so under the same analysis procedure. This difference underscores the presence of quantum correlations, namely quantum entanglement, in Higgs-mediated di-boson decays.

Despite these encouraging observations, one must recall that Bell’s inequality tests face are subject to several well-known loopholes. First, the detection loophole arises because only a fraction of events are recorded [32], although the high efficiency of modern detectors partially mitigates this concern. Second, the locality loophole questions whether particles are sufficiently isolated from classical interactions that could mimic entanglement; robust event selection and particle identification can partially alleviate this concern [10]. Third, the coincidence loophole—the possibility of incorrectly pairing final-state particles—can be addressed by careful momentum reconstruction and by a large ensemble of events, diluting any mislabeling biases [33]. Finally, the freedom-of-choice loophole questions whether measurement choices are truly independent. At a collider, detector configurations are largely fixed, making this the hardest loophole to avoid [34].

Our findings indicate that realistic detector conditions do not appear to significantly obstruct the detection of quantum correlations in Higgs-mediated  $ZZ^*$  decays. We observe robust Bell inequality violations in the signal region, suggesting that such studies are indeed feasible at LHC energies. Future work will aim to improve background modeling, extend the analysis to additional invariant-mass or angular regions where entanglement could be better highlighted, and explore strategies to address the remaining loopholes more definitively (particularly the freedom-of-choice loophole). Although substantial work remains, this study represent a significant step toward demonstrating the viability of probing quantum correlations in high-energy colliders.

## Acknowledgments

The authors thank the ATLAS HZZ Working Group for valuable discussions that helped shape this analysis. We also acknowledge the CMS Collaboration for their commitment to open science and for making their data publicly available, which enabled this independent investigation of quantum entanglement. The authors gratefully acknowledge funding support from the U.S. Department of Energy, Office of Science, under Award DE-FG02-92ER40704.

## References

- [1] Ryszard Horodecki, Pawel Horodecki, Michal Horodecki, and Karol Horodecki. Quantum entanglement. *Rev. Mod. Phys.*, 81:865–942, 2009.

- [2] Nicolas Brunner, Daniel Cavalcanti, Stefano Pironio, Valerio Scarani, and Stephanie Wehner. Bell nonlocality. *Rev. Mod. Phys.*, 86:419, 2014.
- [3] Alain Aspect, Jean Dalibard, and Gerard Roger. Experimental test of Bell’s inequalities using time varying analyzers. *Phys. Rev. Lett.*, 49:1804–1807, 1982.
- [4] J. I. Cirac and P. Zoller. Quantum Computations with Cold Trapped Ions. *Phys. Rev. Lett.*, 74:4091–4094, 1995.
- [5] Alexandre Blais, Ren-Shou Huang, Andreas Wallraff, S. M. Girvin, and R. J. Schoelkopf. Cavity quantum electrodynamics for superconducting electrical circuits: An architecture for quantum computation. *Phys. Rev. A*, 69(6):062320, 2004.
- [6] Alan J. Barr, Marco Fabbrichesi, Roberto Floreanini, Emidio Gabrielli, and Luca Marzola. Quantum entanglement and Bell inequality violation at colliders. *Prog. Part. Nucl. Phys.*, 139:104134, 2024.
- [7] E. Schrodinger. Die gegenwartige Situation in der Quantenmechanik. *Naturwiss.*, 23:807–812, 1935.
- [8] Georges Aad et al. Observation of quantum entanglement in top-quark pairs using the ATLAS detector. 11 2023.
- [9] Aram Hayrapetyan et al. Observation of quantum entanglement in top quark pair production in proton–proton collisions at  $\sqrt{s} = 13$  TeV. *Rept. Prog. Phys.*, 87(11):117801, 2024.
- [10] J. S. Bell. On the Einstein-Podolsky-Rosen paradox. *Physics Physique Fizika*, 1:195–200, 1964.
- [11] Albert Einstein, Boris Podolsky, and Nathan Rosen. Can quantum mechanical description of physical reality be considered complete? *Phys. Rev.*, 47:777–780, 1935.
- [12] M. Fabbrichesi, R. Floreanini, E. Gabrielli, and L. Marzola. Bell inequality is violated in  $B_0 \rightarrow J/\psi K^*(892)0$  decays. *Phys. Rev. D*, 109(3):L031104, 2024.
- [13] Gregor Weihs, Thomas Jennewein, Christoph Simon, Harald Weinfurter, and Anton Zeilinger. Violation of Bell’s inequality under strict Einstein locality conditions. *Phys. Rev. Lett.*, 81:5039–5043, 1998.
- [14] B. Hensen et al. Loophole-free Bell inequality violation using electron spins separated by 1.3 kilometres. *Nature*, 526:682–686, 2015.
- [15] Marissa Giustina et al. Significant-Loophole-Free Test of Bell’s Theorem with Entangled Photons. *Phys. Rev. Lett.*, 115(25):250401, 2015.
- [16] J. A. Aguilar-Saavedra, A. Bernal, J. A. Casas, and J. M. Moreno. Testing entanglement and Bell inequalities in  $H \rightarrow ZZ$ . *Phys. Rev. D*, 107(1):016012, 2023.

- [17] Rachel Ashby-Pickering, Alan J. Barr, and Agnieszka Wierzychucka. Quantum state tomography, entanglement detection and Bell violation prospects in weak decays of massive particles. *JHEP*, 05:020, 2023.
- [18] Albert M Sirunyan et al. Measurements of production cross sections of the Higgs boson in the four-lepton final state in proton–proton collisions at  $\sqrt{s} = 13$  TeV. *Eur. Phys. J. C*, 81(6):488, 2021.
- [19] Gordon L. Kane, G. A. Ladinsky, and C. P. Yuan. Using the Top Quark for Testing Standard Model Polarization and CP Predictions. *Phys. Rev. D*, 45:124–141, 1992.
- [20] W. Bernreuther, A. Brandenburg, Z. G. Si, and P. Uwer. Top quark spin correlations at hadron colliders: Predictions at next-to-leading order QCD. *Phys. Rev. Lett.*, 87:242002, 2001.
- [21] Marco Fabbrichesi, Roberto Floreanini, Emidio Gabrielli, and Luca Marzola. Bell inequalities and quantum entanglement in weak gauge boson production at the LHC and future colliders. *Eur. Phys. J. C*, 83(9):823, 2023.
- [22] Yoav Afik and Juan Ramón Muñoz de Nova. Entanglement and quantum tomography with top quarks at the LHC. *Eur. Phys. J. Plus*, 136(9):907, 2021.
- [23] Yoav Afik and Juan Ramón Muñoz de Nova. Quantum information with top quarks in QCD. *Quantum*, 6:820, 2022.
- [24] Yoav Afik and Juan Ramón Muñoz de Nova. Quantum Discord and Steering in Top Quarks at the LHC. *Phys. Rev. Lett.*, 130(22):221801, 2023.
- [25] Alan J. Barr, Pawel Caban, and Jakub Rembieliński. Bell-type inequalities for systems of relativistic vector bosons. *Quantum*, 7:1070, 2023.
- [26] Qi Bi, Qing-Hong Cao, Kun Cheng, and Hao Zhang. New observables for testing Bell inequalities in W boson pair production. *Phys. Rev. D*, 109(3):036022, 2024.
- [27] Daniel Collins, Nicolas Gisin, Noah Linden, Serge Massar, and Sandu Popescu. Bell Inequalities for Arbitrarily High-Dimensional Systems. *Phys. Rev. Lett.*, 88(4):040404, 2002.
- [28] Dagomir Kaszlikowski, L. C. Kwek, Jing-Ling Chen, Marek Żukowski, and C. H. Oh. Clauser-horne inequality for three-state systems. *Phys. Rev. A*, 65:032118, Feb 2002.
- [29] Paul Langacker. *The Standard Model and Beyond*. Series in High Energy Physics, Cosmology, and Gravitation. CRC Press, Taylor & Francis Group, Boca Raton, FL, 2nd edition, 2021.
- [30] Stefan Wunsch. SMHiggsToZZTo4L dataset in reduced NanoAOD format for education and outreach. CERN Open Data Portal, 2021. Accessed: November 21, 2024.
- [31] Stefan Wunsch. ZZTo2e2mu dataset in reduced NanoAOD format for education and outreach. CERN Open Data Portal, 2021. Accessed: November 21, 2024.



- [32] Philip M. Pearle. Hidden-variable example based upon data rejection. *Phys. Rev. D*, 2:1418–1425, 1970.
- [33] Jan-Åke Larsson and Richard Gill. Bell’s inequality and the coincidence-time loophole. *EPL*, 67:707–713, 2004.
- [34] D. Bohm and Y. Aharonov. Discussion of Experimental Proof for the Paradox of Einstein, Rosen, and Podolsky. *Phys. Rev.*, 108:1070–1076, 1957.